Available online at www.sciencedirect.com
SCIENCE DIRECT®
Journal of Solid State Chemistry 175 (2003) 353–358
JOURNAL OF SOLID STATE CHEMISTRY
http://elsevier.com/locate/jssc

Metal–ligand bonding and rutile- versus CdI_2-type structural preference in platinum dioxide and titanium dioxide

C. Soulard,[a] X. Rocquefelte,[a] S. Jobic,[a,*] D. Dai,[b] H.-J. Koo,[b] and M.-H. Whangbo[b,*]

[a] *Laboratoire de Chimie des Solides, Institut des Matériaux Jean Rouxel, UMR 6502, 2 rue de la Houssinière, B.P. 32229, 44322 Nantes Cedex 03, France*

[b] *Department of Chemistry, North Carolina State University, Raleigh, NC 27695-8204, USA*

Received 24 February 2003; received in revised form 15 May 2003; accepted 30 May 2003

Abstract

First principles electronic structure calculations were carried out to determine the relative stabilities of the rutile- and CdI_2-type structures of platinum dioxide (PtO_2) and titanium dioxide (TiO_2). The orbital interactions between the transition metal *d*- and oxygen *p*-orbitals were analyzed to gain insight into why PtO_2 has both the rutile- and CdI_2-type structures, but TiO_2 has only the rutile-type structure. The cause for the large difference in the *c*/*a* ratios of the CdI_2-type structures of TiO_2 and PtO_2 was examined.

1. Introduction

What electronic factors are responsible for a transition metal dioxide MO_2 to adopt a three-dimensional (3D) or a two-dimensional (2D) layered structure is an interesting and important question. The rutile-type structure is one of several 3D structures that MO_2 can have. In this structure the MO_6 octahedra form edge-sharing MO_4 chains Fig. 1a, these chains are condensed such that the apical oxygen atoms of one MO_4 chain become the equatorial oxygen atoms of two adjacent MO_4 chains Fig. 1b, and every four MO_4 chains form a 1D channel Fig. 1c. In the CdI_2-type layered structure, edge-sharing MO_6 octahedra Fig. 2a form MO_2 layers, and these layers are stacked to form a 3D structure Fig. 2b so that the sheets of oxygen atoms face each other between the layers. Platinum dioxide (PtO_2) has both the CdI_2-type (α-PtO_2, regular form) [1] and the rutile-type (β-PtO_2, high-pressure form) [2] structures, whereas titanium dioxide (TiO_2) has only the rutile structure [3].

Binary oxides of highly electropositive transition metal elements are strongly ionic and adopt 3D structures in which repulsion between O^{2-} anions is reduced. Low-dimensional oxide structures are stabilized by separating O^{2-} anions with counter cations (e.g., Na_xCoO_2, $K_{0.3}MoO_3$, etc.) or by use of transition elements with high oxidation state (e.g., MoO_3, V_2O_5, etc.) [4]. Thus, it is understandable that TiO_2 has only a 3D structure because of the large electronegativity difference between Ti and O (1.54 vs. 3.44). The driving force to adopt a 3D structure would be weaker in PtO_2 due to the smaller electronegativity difference between Pt and O (2.28 vs. 3.44). Nevertheless, one may wonder why PtO_2 can have a 2D layered structure despite the expected enhancement of anion–anion repulsion. It should be noted that a CdI_2-type layered structure is also found for metastable CoO_2 and NiO_2 phases obtained by electrochemical deintercalation of lithium from $LiNi_{1-x}Co_xO_2$ [5,6].

The electronic structures and chemical bonding of rutile-type compounds have been analyzed on the basis of electronic band structure calculations [7]. There are several 3D polymorphs of a transition metal binary oxide MO_2, which include the rutile-, $CaCl_2$-, marcasite- and anatase-type phases. The relative stabilities of these 3D polymorphs and the mechanism for the phase transition between them are important issues. Answers to these questions have been provided for a few oxides in terms of electronic band structure studies [8,9]. In the present work, we probe why both rutile- and CdI_2-type (i.e., 3D and 2D) structures are possible for PtO_2 while the CdI_2-type structure is not feasible for TiO_2 on the basis of first principles electronic structure calculations.

*Corresponding author. Fax: +1-919-515-7832.
E-mail addresses: stephane.jobic@cnrs-imn.fr (S. Jobic), mike_whangbo@ncsu.edu (M.-H. Whangbo).

0022-4596/03/$ - see front matter © 2003 Elsevier Inc. All rights reserved.
doi:10.1016/S0022-4596(03)00323-2

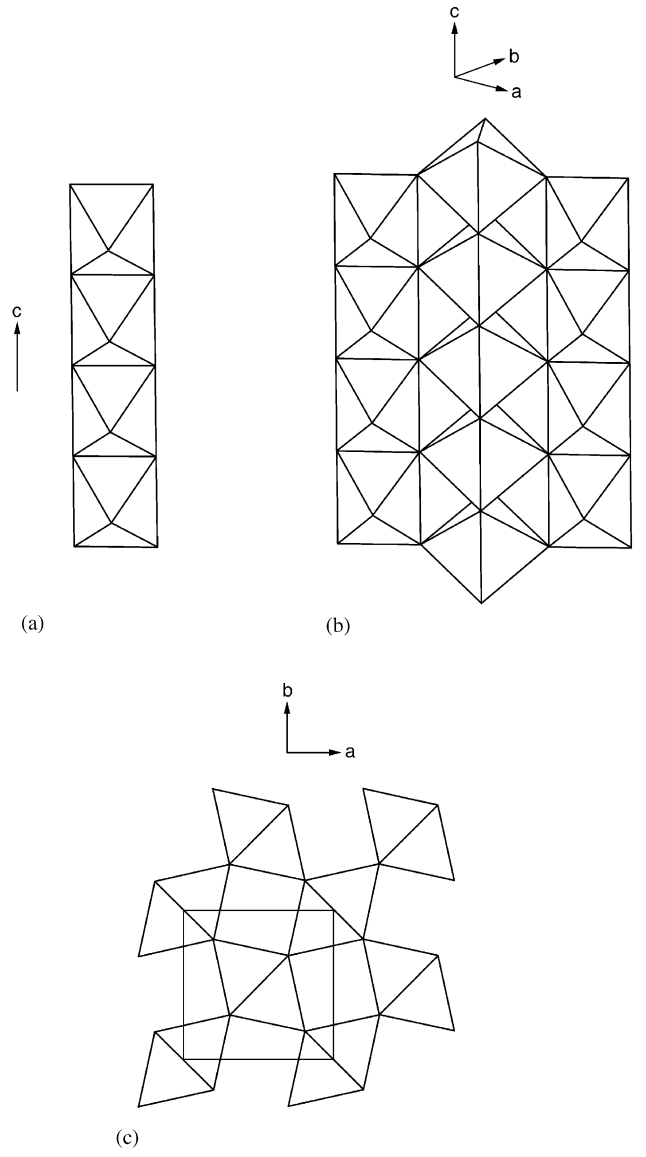

Fig. 1. Rutile-type MO_2 structure: (a) Schematic polyhedral view of a single MO_4 chain made up of edge-sharing MO_6 octahedra. (b) Schematic polyhedral view of how MO_4 chains condense in the rutile-type structure of MO_2. (c) Projection view of MO_4 chains along the chain direction.

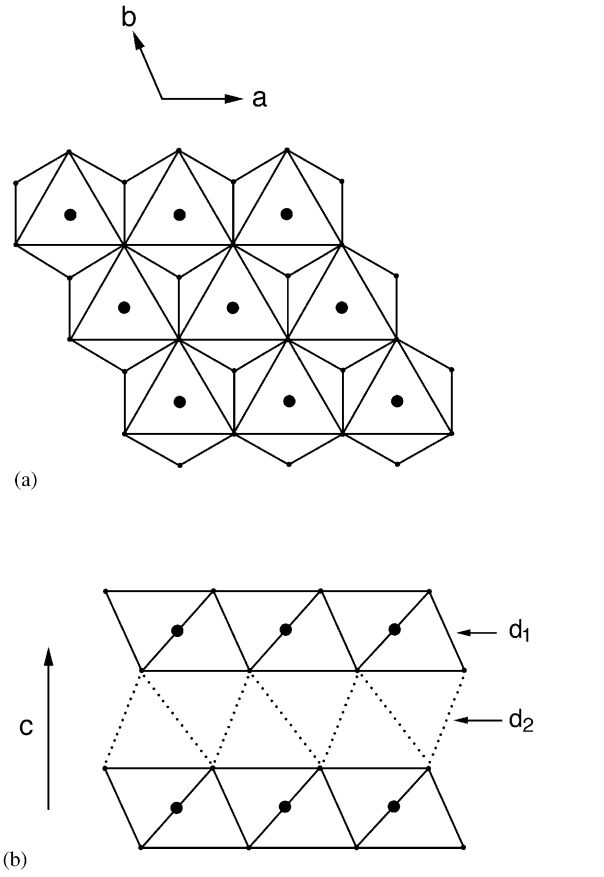

Fig. 2. CdI_2-type MO_2 structure: (a) Schematic projection view of a single MO_2 layer along the c-direction. (b) Schematic perspective view of adjacent MO_2 layers in the CdI_2-type structure of MO_2.

To gain insight into what electronic features are responsible for the structural and electronic difference between PtO_2 and TiO_2, we then analyze the orbital interactions between the transition metal d- and oxygen p-orbitals.

2. Calculations

The cell parameters and the atom positions for the rutile- and CdI_2-type structures of PtO_2 and TiO_2 were optimized on the basis of electronic band structure calculations using the Vienna ab initio simulation package (VASP) [10–12], which is based on the density functional theory within the local-density approximation. The present VASP calculations employed the projector augmented wave method [13], a finite temperature density functional approximation, an optimized mixing routine and a conjugate gradient scheme. All calculations were performed using the generalized-gradient approximation [14].

First principles full potential linearized plane wave (FP-LAPW) calculations with non-spin polarization were carried out for the rutile and CdI_2 structures of PtO_2 and TiO_2 (determined from the VASP calculations) using the WIEN2k program package [15] within the generalized-gradient approximation [16] for the exchange-correlation energy. We employed the muffin–tin radii of 2.32 au for Pt, 2.19 au for Ti, and 1.56 au for O. The basis set cut-off parameters were $G_{max} = 14\,\text{Bohr}^{-1}$ and $R_{mt}K_{max} = 7$ (G_{max} controls the plane wave cut-off used in the charge density Fourier expansion, and $R_{mt}K_{max}$ defines the plane wave basis set used to describe the wave function outside the muffin–tins). Integrations over the irreducible wedge of

the Brillouin zone were performed using a 2500k-point regular mesh.

3. Results

The structural data determined by VASP calculations are summarized in Table 1a-d, where the experimental values of the cell parameters and atom coordinates of the observed structures of PtO_2 and TiO_2 are given in parentheses. The structures optimized by VASP calculations are in good agreement with the available experimental data. It is noted that in Ref. [1], the z coordinate of O in α-PtO_2 was not experimentally determined but was arbitrary fixed at $\frac{1}{4}$.

The relative energies of the rutile- and CdI_2-type structures for PtO_2 and TiO_2 (per formula unit) determined by VASP calculations are listed in Table 2, which also lists the relative energies determined by FP-LAPW calculations for the structures obtained from VASP calculations. The rutile- and CdI_2-type structures are almost equally stable for PtO_2 (the energy difference lies within the computational error, which is estimated to be about 10 meV/atom), but the rutile structure is considerably more stable than the CdI_2-type structure for TiO_2. These results are consistent with the experimental observations that PtO_2 has the CdI_2- and rutile-type structures, while TiO_2 has only the rutile structure.

Fig. 3 shows the total density of states (DOS) and the partial DOS of the metal d-orbitals obtained for the rutile- and CdI_2-type structures of TiO_2 using FP-LAPW calculations. The corresponding DOS plots for the rutile- and CdI_2-type structures of PtO_2 are shown in Fig. 4. In capturing the essential features of these DOS plots, it is convenient to consider the oxidation states of the metal atoms. With the oxidation state O^{2-} for oxygen, the oxidation states for platinum and titanium are given by Pt^{4+} (d^6) and Ti^{4+} (d^0), respectively. This ionic electron counting scheme predicts that both the t_{2g}- and e_g-block bands are empty in TiO_2, and that the t_{2g}bands are completely filled but the e_g-block bands are empty in PtO_2. These predictions are consistent with the total and partial DOS plots shown in Figs. 3 and 4.

Fig. 3 shows that the t_{2g}- and e_g-block bands of TiO_2 are well separated in energy in the CdI_2-type structure, but almost overlap in the rutile structure because they are wider in the rutile structure than in the CdI_2-type structure. The DOS for the occupied bands of TiO_2 is wider and has a more even distribution in the rutile structure than in the CdI_2-type structure. Fig. 4 shows

Table 1
Crystal structures of the rutile- and CdI_2-type structures of PtO_2 and TiO_2 determined by VASP calculations[a]

(a)Rutile-type PtO_2[b]
SG: *Pnnm*; $a = 4.5986$ (*4.488*) Å, $b = 4.5717$ (*4.533*) Å, $c = 3.1910$ (*3.138*) Å
Atom coordinates: Pt (0, 0, 0); O (0.2571 (*0.2670*), 0.3633 (*0.3500*), 0)

(b) CdI_2-type PtO_2[c]
SG: $P\bar{3}m1$; $a = 3.1644$ (*3.100*) Å, $c = 4.3241$ (*4.161*) Å
Atom coordinates: Pt (0, 0, 0); O (1/3, 2/3, 0.2190 (*0.25*[d]))

(c) Rutile-type TiO_2[e]
SG: $P4_2/mnm$; $a = 4.6536$ (*4.5937*) Å, $c = 2.9713$ (*2.9587*) Å
Atom coordinates: Ti (0, 0, 0), (1/2, 1/2, 1/2); O (x, x, 0), ($1/2+x$, $1/2-x$, 1/2) with $x = 0.3044$ (*0.30499*)

(d) CdI_2-type TiO_2
SG: $P\bar{3}m1$; $a = 2.9962$ Å, $c = 5.0806$ Å
Atom coordinates: Ti (0, 0, 0); O (1/3, 2/3, 0.1923)

[a] The experimental values are given in italics in parentheses.
[b] The experimental structure was taken from Ref. [2].
[c] The experimental structure was taken from Ref. [1].
[d] The assumed value.
[e] The experimental structure was taken from Ref. [3].

Table 2
Relative energies (eV) per formula unit determined by VASP and WIEN2k calculations for the rutile- and CdI_2-type structures of PtO_2 and TiO_2[a]

Compound	Structure type	VASP	WIEN2k
PtO_2	Rutile	0.000	0.000
	CdI_2	0.067	0.013
TiO_2	Rutile	0.000	0.000
	CdI_2	0.339	0.350

[a] For each compound, the energy of the rutile structure was taken as the reference.

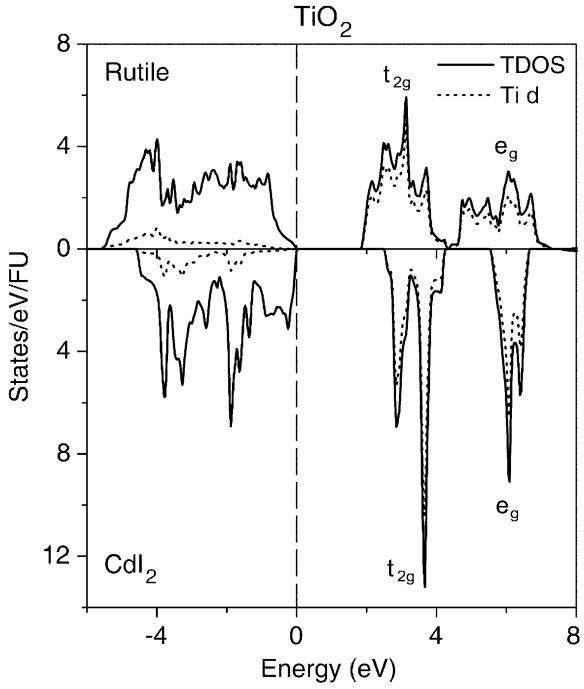

Fig. 3. Plots of the total DOS (solid line) and the Ti 3*d*-orbital contributions (dashed line) calculated for the rutile- and CdI_2-type structures of TiO_2 obtained by FP-LAPW calculations.

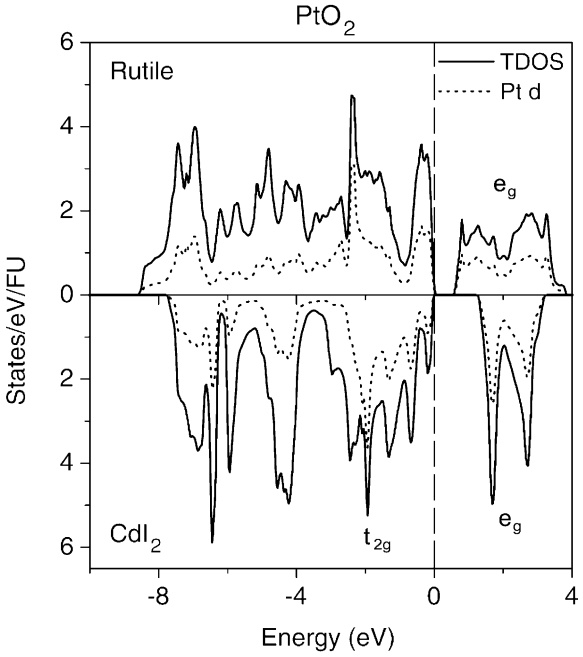

Fig. 4. Plots of the total DOS (solid line) and the Pt 5*d*-orbital contributions (dashed line) calculated for the rutile- and CdI_2-type structures of PtO_2 obtained by FP-LAPW calculations.

that the e_g-block bands of PtO_2 are wider in the rutile-type structure than in the CdI_2-type structure. The DOS for the occupied bands of PtO_2 is wider and has a more even distribution in the rutile structure than in the CdI_2-type structure. For the CdI_2-type structure of PtO_2, the t_{2g}-block bands can be assigned to the energy region between -3 and 0 eV. Such an assignment is not possible for the rutile-type structure of PtO_2, because the *d*-orbital contribution is more evenly distributed in the occupied energy region and because the oxygen *s*/*p*-block bands are merged with the platinum t_{2g}-block bands. It is clear from the DOS curves of Figs. 3 and 4 that the mixing between the metal *d*-orbitals and the oxygen *s*/*p*-orbitals is much stronger in PtO_2 than in TiO_2.

4. c/a ratios for the CdI_2-type structures of MO_2 (M = Ti, Pt)

Some geometrical parameters for the CdI_2-type structures of MO_2 (M = Ti, Pt) are summarized in Table 3. Our calculations reproduce the low c/a ratio of PtO_2 ($\sim$1.34), and the high c/a ratio ($\sim$1.67) expected for TiO_2 on the basis of hexagonal close packing of O^{2-} anions. These results are consistent with the experimental observations for the corresponding layered sulfides, i.e., $c/a = 1.42$ for PtS_2 [17] and $c/a = 1.67$ for TiS_2 [18]. Our recent study [19] showed that the small c/a value in the CdI_2-type PtO_2's and dichalcogenides PtQ_2 (Q = O, S, Se, Te) is primarily caused by the overlap repulsion between the in-plane *np*-orbitals of Q within each sheet of the ligand atoms Q, i.e., the two-orbital four-electron destabilizing orbital interaction [20] between the filled in-plane *np*-orbitals. Thus, a smaller Pt–Q bond results in a smaller c/a ratio [19].

To understand the large difference in the c/a ratios of TiO_2 and PtO_2, we examine the intra-layer O···O (between sheets of oxygen atoms) distance d_1 and the inter-layer O···O distance d_2 Fig. 2, Table 3. The d_1/a ratios of TiO_2 and PtO_2 are both smaller than 1 (i.e., 0.869 and 0.832, respectively), namely, both TiO_6 and PtO_6 octahedra are squashed along the *c*-axis. The extent of this flattening is only slightly larger in PtO_2. However, the d_2/a ratio is much larger in TiO_2 than in PtO_2 (i.e., 1.208 vs. 0.961). Thus, the primary cause for the large c/a ratio of TiO_2 and the small c/a ratio of PtO_2 lies in the fact that the inter-layer O···O distance

Table 3
Geometrical parameters in the CdI_2-type structures of MO_2 (M = Ti, Pt) obtained by VASP calculations[a]

	TiO_2	PtO_2
M–O	1.984	2.058
a	2.996	3.164
d_1 (intra-layer O···O)	2.602	2.632
d_2 (inter-layer O···O)	3.582	3.040
c/a	1.696	1.366
d_1/a	0.869	0.832
d_2/a	1.208	0.961

[a] Lengths are given in Å.

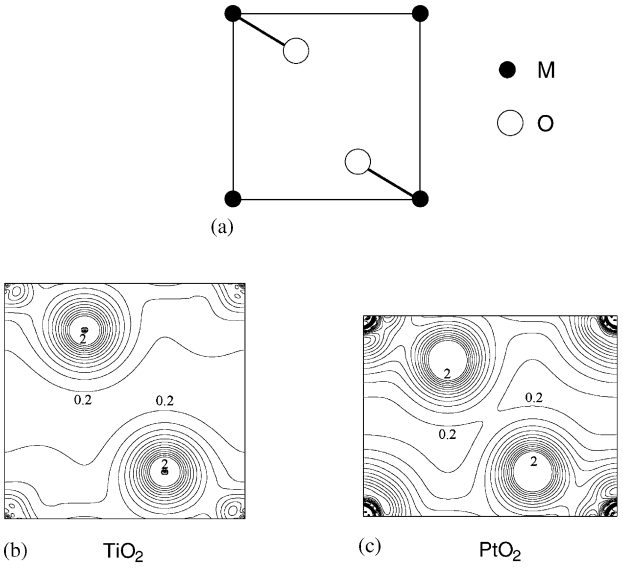

Fig. 5. (a) Schematic diagram shown a cross-section plane of the CdI_2-type structure of MO_2 (M = Ti, Pt) that is parallel to the (110) plane and contains *M*–O bonds. The contour plots of the valence electronic density distribution on this plane calculated for TiO_2 and PtO_2 are shown in (b) and (c), respectively. The contour values vary from 0.2 $e^-/Å^3$ to 2.0 $e^-/Å^3$ with the interval of 0.15 $e^-/Å^3$.

d_2 is large in TiO_2, but small in PtO_2. To account for this difference, we recall that the Ti–O bond is more strongly ionic than is the Pt–O bond. In terms of electron density distribution, the anionic character of oxygen is much stronger in TiO_2 than in PtO_2. Consequently, the anion–anion repulsion between adjacent sheets of O atoms is stronger in TiO_2 than in PtO_2, so that the CdI_2-type structure of TiO_2 has a larger interlayer spacing and hence a larger c/a ratio. Fig. 5 compares the valence electron density distribution in the CdI_2-type structures of TiO_2 and PtO_2. As expected from the above discussion, Fig. 5 shows that each Pt–O bond has a stronger covalent character than does each Ti–O bond, and the oxygen atom has a stronger ionic character in TiO_2 than in PtO_2.

5. Structural preference and orbital interactions

We now analyze the differences in the structural preference of PtO_2 and TiO_2 from the viewpoint of interactions between the metal d-orbitals and the oxygen p-orbitals. In the rutile-type structure, each oxygen atom and its three adjacent metal atoms form an OM_3 triangle with oxygen at the center Fig. 6a in which $\angle M-O-M = 98.2°$ and $130.9°$ ($\times 2$) from the structure optimized by the VASP calculations for β-PtO_2. In the CdI_2-type structure, each oxygen atom and its three adjacent metal atoms form an OM_3 trigonal pyramid with oxygen at the apex Fig. 6b in which $\angle M-O-M = 99.7°$ ($\times 3$) from the structure optimized by the VASP calculations for α-PtO_2. This structural difference in the local structures around each oxygen atom has a profound consequence on the metal–ligand bonding and structural preference in PtO_2 and TiO_2.

For simplicity, let us suppose that a given trigonal planar OM_3 unit of the rutile-type structure Fig. 6a is contained in the xy-plane with one O–M bond aligned along the x-axis as shown in Fig. 7. Then the xz-orbital of M has a strong π-interaction with the z-orbital of O Fig. 7a, the xy-orbital of M has a strong π-interaction with the y-orbital of O Fig. 7b, and the x^2-y^2-orbital of M has a strong σ-interaction with the x-orbital of O Fig. 7c. By symmetry, the z^2- and yz-orbitals of M cannot interact with the p-orbitals of O Figs. 7d and e. The occurrence of such strong π- and strong

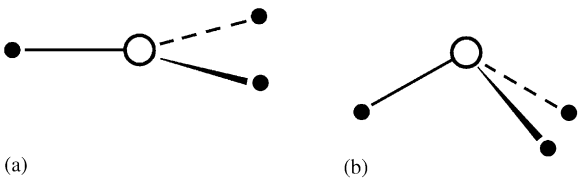

Fig. 6. Local geometry of an OM_3 unit at each oxygen site in the (a) rutile- and (b) CdI_2-type structures of a transition metal dioxide MO_2.

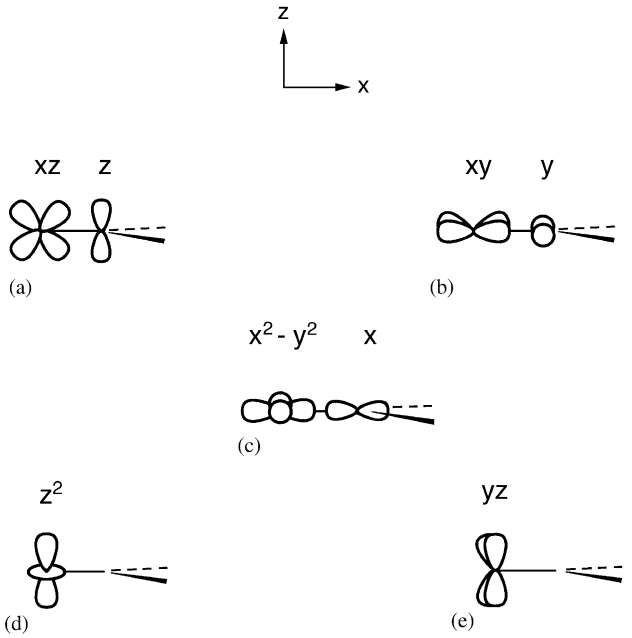

Fig. 7. Overlap between the d-orbitals of M and p-orbitals of O in the rutile-type structure of MO_2.

σ-interactions is energetically favorable when they are two-orbital two-electron stabilizing interactions [15], namely, when the d-orbitals of d^0 ions interact with the p-orbitals of O^{2-} ions. This is the case for the rutile structure of TiO_2. In the trigonal pyramidal OM_3 geometry of the CdI_2-type structure Fig. 6b, each d-orbital of M can interact with one of the p-orbitals of O due to the lowering of the symmetry. The π-interactions involving the xz- and xy-orbitals of M are strongly reduced in strength, and so is the σ-interaction involving the x^2-y^2-orbital of M. The z^2-orbital of M will gain weak σ-interactions with the z and x-orbitals of O, and the yz-orbital of M a weak π-interaction with the y-orbital of O. All these interactions are stabilizing for the case of TiO_2. However, the overall strength of the two-orbital two-electron stabilizing interactions should be much stronger in the rutile structure than in the CdI_2-type structure, because TiO_2 is much more stable in the rutile structure than in the CdI_2-type structure in terms of total energy calculations.

From the viewpoint of the ionic electron counting scheme, each Pt^{4+} ion of PtO_2 has six d-electrons so that not all the orbital interactions of the Pt^{4+} ion d-orbitals with the O^{2-} ion p-orbitals are stabilizing interactions. In the case of the trigonal planar OM_3 geometry of the rutile-type structure Fig. 6a, it should be noted that the π-interactions of Figs. 7a and b lead to the t_{2g}-block bands, and the σ-interaction of Fig. 7c to the e_g-block bands. In the case of PtO_2, the t_{2g}-block bands are filled while the e_g-block bands are empty. Therefore, the two π-interactions of Figs. 7a and b become two-orbital four-electron destabilizing interactions [20], while the

σ-interaction of Fig. 7c is a two-orbital two-electron stabilizing interaction. When the local geometry around oxygen is converted to the trigonal pyramidal OM_3 geometry of the CdI_2-type structure Fig. 6b, the two-orbital four-electron destabilizing π-interactions of Figs. 7a and b are significantly weakened in strength, and so is the two-orbital two-electron stabilizing σ-interaction of Fig. 7c. In addition, the z^2-orbital of Pt^{4+} will induce weak σ-interactions (stabilizing) with the x- and z-orbitals of O^{2-}, and the yz-orbital of Pt^{4+} a weak π-interaction (destabilizing) with the y-orbital of O^{2-}. Namely, PtO_2 has strong destabilizing π- and strong stabilizing σ-interactions in the rutile-type structure, while these interactions are reduced in strength in the CdI_2-type structure. Therefore, there will be no strong structural preference between the rutile- and CdI_2-type structures in the case of PtO_2. This is consistent with the experimental and theoretical observations.

Finally, it is noted that the DOS for the occupied bands of TiO_2 is wider, and the t_{2g}- and e_g-block bands of TiO_2 are wider, in the rutile structure than in the CdI_2-type structure because the π- and σ-interactions are stronger in the rutile-type structure Fig. 3. The same is also found for PtO_2 Fig. 4. The energy difference between the Pt 5*d*- and O 2*p*-orbital is smaller than that between the Ti 3*d*- and O 2*p*-orbitals, so that the orbital interactions between them are stronger in PtO_2. This explains why the partial DOS for the Pt 5*d*-orbitals is distributed almost evenly in the occupied region.

6. Concluding remarks

Our first principles electronic structure calculations reveal that the rutile- and CdI_2-type structures are almost equally stable for PtO_2, but the rutile structure is considerably more stable than the CdI_2-type structure for TiO_2. These results are consistent with the available experimental observations. Our analysis of orbital interactions shows that PtO_2 has strong destabilizing π- and strong stabilizing σ-interactions in the rutile-type structure, and both interactions are reduced in strength in the CdI_2-type structure such that there is no strong structural preference between the rutile- and CdI_2-type structures in the case of PtO_2. The primary cause for making the CdI_2-type structure accessible for PtO_2 is that the t_{2g}-block levels of each transition metal ion are occupied. A similar situation occurs in the metastable NiO_2 and CoO_2 phases obtained by the electrochemical deintercalation of lithium from $LiNi_{1-x}Co_xO_2$, which are found to crystallize in the CdI_2-type layered structure. The c/a ratio of the CdI_2-type structure is much larger in TiO_2 than in PtO_2 because the anionic character of oxygen is much stronger in TiO_2 than in PtO_2 so that the anion–anion repulsion between adjacent sheets of O atoms is stronger in TiO_2 than in PtO_2. Thus, the present work indicates that the stabilization of lamella oxides of transition element is feasible if the M–O bond is substantially covalent, which occurs for late transition elements. As discussed above, such oxides have a delicate balance between metal–oxygen and oxygen–oxygen orbital interactions, and hence their synthesis would require soft chemistry routes.

Acknowledgments

Work at North Carolina State University was supported by the Office of Basic Energy Sciences, Division of Materials Sciences, US Department of Energy, under Grant DE-FG02-86ER45259. The authors are grateful to North Carolina Supercomputer Center for the generous computer time.

References

[1] H.R. Hoekstra, S. Siegel, F.X. Gallagher, Adv. Chem. Ser. 98 (1971) 39.
[2] K.-J. Range, F. Rau, U. Klement, A.M. Heyns, Mater. Res. Bull. 22 (1987) 1541.
[3] K. Sugiyama, Y. Takeuchi, Z. Kristallogr. 194 (1991) 305.
[4] J. Rouxel, T. Bein (Ed.), Supramolecular architecture: synthetic control, in: Thin Films and Solids ACS Symposium Series, Vol. 499, American Chemical Society, Washington, DC, 1992, pp. 88–113.
[5] J.M. Tarascon, G. Vaughan, Y. Chabre, L. Seguin, M. Anne, P. Strobel, G. Amatucci, J. Solid State Chem. 147 (1999) 410.
[6] L. Croguennec, C. Pouillerie, A.N. Mansour, C. Delmas, J. Mater. Chem. 11 (2001) 131.
[7] P.I. Sorantin, K. Schwarz, Inorg. Chem. 31 (1992) 567.
[8] J.K. Burdett, T. Hughbanks, G.J. Miller, J.W. Richardson Jr., J.V. Smith, J. Am. Chem. Soc. 109 (1987) 3639.
[9] R. Wu, W.H. Weber, J. Phys.: Condens. Matter 12 (2000) 6725.
[10] G. Kresse, J. Furthmüller, Vienna Ab-initio Simulation Package (VASP), Institut für Materialphysik, Universität Wien, Austria. See also: http://cms.mpi.univie.ac.at/VASP/.
[11] G. Kresse, J. Furthmüller, Comput. Sci. 6 (1996) 15.
[12] G. Kresse, J. Furthmüller, Phys. Rev. B 54 (1996) 11169.
[13] P.E. Blöchl, Phys. Rev. B 50 (1994) 17953;
G. Kresse, D. Joubert, Phys. Rev. B 59 (1999) 1758.
[14] J.P. Perdew, Y.Y. Wang, Phys. Rev. B 33 (1986) 8800.
[15] P. Blaha, K. Schwarz, G. Madsen, D. Kvasnicka, J. Luitz, WIEN2k, An Augmented Plane Wave + Local Orbitals Program for Calculating Crystal Properties, Karlheinz Schwarz, Techn. Universität Wien, Austria, 2001. ISBN 3-9501031-1-2. See also: http://www.wien2k.at/
[16] J.P. Perdew, S. Burke, M. Ernzerhof, Phys. Rev. Lett. 77 (1996) 3865.
[17] S. Furuseth, K. Selte, A. Kjekshus, Acta Chem. Scand. 19 (1965) 257.
[18] R.R. Chianelli, J.C. Scanlon, A.H. Thompson, Mater. Res. Bull. 10 (1974) 1379.
[19] T.A. Albright, J.K. Burdett, M.-H. Whangbo, Orbital Interactions in Chemistry, Wiley, New York, 1985 (Chapter 2).
[20] D. Dai, H.-J. Koo, M.-H. Whangbo, C. Soulard, X. Rocquefelte, S. Jobic, J. Solid State Chem. 173 (2003) 114.